Atmos. Meas. Tech. Discuss., https://doi.org/10.5194/amt-2019-164
Manuscript under review for journal Atmos. Meas. Tech.
Discussion started: 10 May 2019

Atmospheric Measurement Techniques Discussions

A New Instrument for Time Resolved Measurement of HO_2 Radicals

Thomas H. Speak[1], Mark A. Blitz[1,2]*, Daniel Stone[1] and Paul W. Seakins[1,2]*

1 – School of Chemistry, University of Leeds, Leeds, LS2 9JT, UK

2 – National Centre for Atmospheric Science, Leeds, LS2 9JT, UK

Abstract

OH and HO_2 radicals are closely coupled in the atmospheric oxidation and combustion of volatile organic compounds (VOCs). Simultaneous measurement of HO_2 yields and OH kinetics can provide the ability to assign site specific rate coefficients that are important for understanding the oxidation mechanisms of VOCs. By coupling a FAGE LIF detection system for OH and HO_2 with a high pressure laser flash photolysis system, it is possible to accurately measure OH pseudo-first-order loss processes up to ~100000 s^{-1} and to determine HO_2 yields via time resolved measurements. This time resolution allows discrimination between primary HO_2 from the target reaction and secondary production from side reactions. The apparatus was characterized by measuring yields from the reactions of OH with H_2O_2 (1:1 link between OH and HO_2), with C_2H_4/O_2 (where secondary chemistry can generate HO_2), with C_2H_6/O_2 (where there should be zero HO_2 yield) and with CH_3OH/O_2 (where there is a well-defined HO_2 yield).

As an application of the new instrument, the reaction of OH with n-butanol has been studied at 293 and 616 K. The bimolecular rate coefficient at 293 K, $(9.24 \pm 0.21) \times 10^{-12}$ cm^3 $molecule^{-1}$ s^{-1}, is in good agreement with recent literature, verifying that this instrument can both measure HO_2 yields and accurate OH kinetics. At 616 K the regeneration of OH in the absence of O_2, from the decomposition of the β-hydroxy radical, was observed, which allowed the determination of the fraction of OH reacting at the β site (0.23 ± 0.04). Direct observation of the HO_2 product in the presence of oxygen has allowed the assignment of the α-branching fractions (0.57 ± 0.06) at 293 K and (0.54 ± 0.04) at 616 K); branching ratios are key to modelling the ignition delay times of this potential 'drop-in' biofuel.

1 Introduction

In the atmosphere, HO_2 and OH radicals (OH + HO_2 = HOx) are closely coupled via several reactions as shown in Scheme 1. The short lifetimes of HOx radicals mean that concentrations are determined by chemical production and removal and not by transport processes, making them ideal candidates as test species for our understanding of atmospheric chemical mechanisms (Stone et al., 2012;Monks, 2005;Stockwell et al., 2012).

Atmos. Meas. Tech. Discuss., https://doi.org/10.5194/amt-2019-164
Manuscript under review for journal Atmos. Meas. Tech.
Discussion started: 10 May 2019

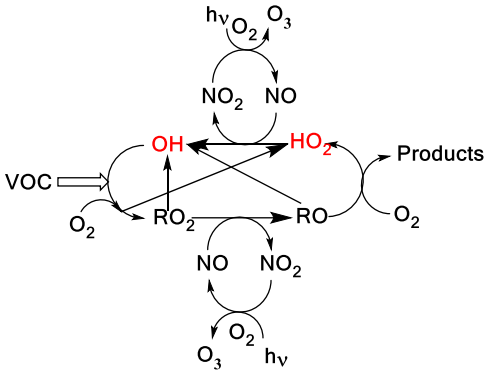

Scheme 1. A simplified tropospheric HOx cycle showing the importance of these short-lived radical species both to the chemical removal of VOCs and the formation of ozone.

In Scheme 1, the reaction of alkoxy radicals with molecular oxygen is a major route to HO_2 formation; however, this is not the only significant HO_2 formation process; for example, in the atmospheric oxidation of n-butanol, HO_2 can be formed via two different mechanisms. Abstraction by OH at the α position leads to a radical which reacts with oxygen to directly produce HO_2 (R1a, R2) whereas abstraction at other sites leads to alkylperoxy radical ($C_4H_9O_2$) formation with varying fractions of the RO_2 forming alkoxy radicals, and subsequently HO_2 (McGillen et al., 2013) on a longer timescale.

$$OH + CH_3CH_2CH_2CH_2OH \rightarrow CH_3CH_2CH_2CHOH + H_2O \quad \text{(R1a)}$$

$$CH_3CH_2CH_2CHOH + O_2 \rightarrow HO_2 + CH_3CH_2CH_2CHO \quad \text{(R2)}$$

The fraction of alkoxy radicals formed depends on the mechanism of RO_2 removal (reaction with NO or self or cross-reactions) and the yield of HO_2 from the alkoxy radical depends on the competition between decomposition, isomerization and reaction with O_2, which in turn will depend on the structure of the alkoxy radical, temperature, pressure and concentration of oxygen (Orlando et al., 2003). Therefore, in order to determine the HO_2 yield from the OH initiated oxidation of compounds such as n-butanol, it is important to have a selective, sensitive and time resolved method of HO_2 detection.

The importance of HO_2 chemistry is not limited to atmospheric processes; HO_2 is a key intermediate in low temperature (500 – 1000 K) combustion processes, particularly those involving

oxygenated fuels (Zador et al., 2011). The mechanisms of low temperature combustion are of particular interest in the development of new engine technologies such as reactively controlled compression ignition (RCCI) (Reitz and Duraisamy, 2015) and are closely linked to atmospheric oxidation mechanisms. Monitoring HO_2 concentrations under the elevated temperatures and high pressures of combustion processes is therefore also of interest. In low-temperature combustion, HO_2 formation is a chain inhibition process, with OH reformation a chain propagating or chain branching process. The ratio of chain branching to chain inhibition processes is often the controlling factor in modelling ignition delay times (Agbro et al., 2017). High temperatures and concentrations of oxygen may be required to convert atmospheric processes, which take several 10s of seconds at ambient temperatures (and hence may be influenced by surface chemistry or secondary reactions) to the milli- or microsecond timescale where they can be studied by flash photolysis techniques without such interferences (Medeiros et al., 2018).

Direct measurements of HO_2 rely on absorption techniques, and kinetic information on HO_2 reactions has been determined mainly using absorption spectroscopy. This can be achieved either with conventional absorption techniques, often in the UV, (including multipass optics to enhance the pathlength) or in the IR with cavity ring down spectroscopy (CRDS) (Assaf et al., 2018;Onel et al., 2017). However, the HO_2 UV absorption spectrum (200 - 260 nm) is broad and featureless (Crowley et al., 1991), and as such, overlaps with the UV absorptions of many other species present in atmospheric degradation pathways or combustion systems (particularly H_2O_2 and RO_2). To utilize the selectivity of the structured IR spectra, absorption methods have been developed in both the mid and near-IR (NIR) (Taatjes and Oh, 1997). Mid-IR absorption features for HO_2 provide sufficient absorption cross-sections for study (Jemialade and Thrush, 1990) but suffer from severe pressure broadening, reducing sensitivity under the conditions relevant to atmospheric and combustion systems (Thiebaud and Fittschen, 2006). Detection in the NIR has similar advantages in terms of a structured spectrum providing greater selectivity; the weaker absorption cross-sections are compensated by the higher powers and ease of use of NIR laser sources (Gianella et al., 2016). However, pressure broadening and interference from H_2O absorptions can make these measurements difficult at even low concentrations of water (10^{14} molecule cm^{-3}).

Atmos. Meas. Tech. Discuss., https://doi.org/10.5194/amt-2019-164
Manuscript under review for journal Atmos. Meas. Tech.
Discussion started: 10 May 2019

In the atmosphere (Stone et al., 2012) and in chamber studies (Glowacki et al., 2007), HO_2 is detected using a sensitive, but indirect method via conversion to OH, with detection of OH via laser induced fluorescence (LIF) (Hard et al., 1984;Brune et al., 1995;Fuchs et al., 2011) or conversion to $H_2{}^{34}SO_4$ with subsequent detection of the acid via mass spectrometry (Edwards et al., 2003;Hanke et al., 2002). In the LIF method, also known as Fluorescence Assay by Gaseous Expansion (FAGE (Hard et al., 1984)), which is the technique used in this study, OH is sampled into a low pressure region through a pinhole. Low pressures allow for the temporal separation of resonant 308 nm fluorescence from the excitation pulse. Following the first detection axis for OH, a flow of NO is introduced which reacts with HO_2 (R3):

$$HO_2 + NO \rightarrow OH + NO_2 \qquad \text{(R3)}$$

The resulting OH is monitored at a second detector. The high sensitivity with which OH can be detected gives HO_2 detection limits in the 10^8 molecule cm^{-3} range for 5 – 10 s averaging, however, to extract concentrations, both OH detection methods require calibration (Winiberg et al., 2015). For chamber measurements of HO_2, comparisons with direct CRDS measurements have verified the reliability of the calibration process (Onel et al., 2017).

HO_2 detection by LIF can be potentially sensitive to interferences from certain RO_2 species which may also be converted to OH on short timescales. Interferences can be minimized by short conversion times between NO injection and OH monitoring, utilizing low pressures, high flow rates of the sample gas, and low NO concentrations to separate OH generation from HO_2 and RO_2, reduced conversion of HO_2 reduces the sensitivity of this technique and as such in practice a compromise between selectivity and sensitivity is used (Fuchs et al., 2011;Hard et al., 1984;Whalley et al., 2013).

The current paper describes a significant development on our earlier FAGE based instrument for time-resolved OH detection (Stone et al., 2016). In this improved system, laser flash photolysis in a high pressure (up to 5 bar), temperature controllable (300 – 800 K) reactor (shown in Figure 1) generated radicals which were then sampled through a pinhole forming a jet within the low pressure detection region (shown in more detail in Figure 2). OH radicals were monitored by LIF close to the pinhole. The jet breaks down after ~20 mm and NO was injected after this point to convert some HO_2 into OH which was then detected by a second monitoring system. In general, LIF becomes less sensitive at higher temperatures (due to distribution of population over

more rotational levels) and O_2 concentrations (due to quenching). Sampling into the low-pressure region reduces both the effect of collisional quenching and temperature on the sensitivity of LIF detection, although there is a reduction in the number density of the HOx species in the expansion. We report the adaptation of our time-resolved OH-FAGE instrument to allow HO_2 detection, the characterization of the instrument (including development of a calibration method for HO_2 yields of OH initiated reactions), and the investigation of the influence of RO_2 species. Finally, we discuss the application of the technique to determine the yield of HO_2 from the reaction of OH with n-butanol.

2 Experimental

Reactions were carried out in a high pressure (0.5 – 5 bar) reaction cell which is described in greater detail in Stone et al. (2016) and schematics of which are shown in Figures 1 and 2. The high-pressure reactor was a 0.5 m stainless steel tube with a 22 mm internal diameter. Gas flows were delivered to the high-pressure cell from a mixing manifold where calibrated mass flow controllers (MFC) allowed for accurate control of flow rates. Low vapour pressure compounds: OH precursors (H_2O_2), and substrates methanol and butanol, were delivered to the mixing manifold from, thermostatted bubblers in pressure regulated backing flows of nitrogen (N_2). Ethane and oxygen were delivered directly from cylinders into the mixing manifold through MFCs. The gas flowrate through the cell was kept under laminar conditions with typical Reynolds values (Re) of 480 (corresponding to a flow rate for an experiment of 10 SLM at 2 bar); in general conditions were maintained between 400-800 Re (Re < 2400 = laminar flow), with some experiments carried out with higher flowrates, up to 1800 Re.

Temperature control of the reactor between room temperature and 800 K was achieved by altering the voltage applied to a coil heater (WATROD tubular heater, Watlow) over the last 30 cm of the stainless-steel tube. The heated region was fitted with a quartz liner (inner diameter 18 mm) to reduce wall-initiated chemistry. A temperature readout, from a type K thermocouple in the gas flow, close to the pinhole, was calibrated for given flow rates, pressures and voltage settings by measuring the highly temperature sensitive OH and methane rate coefficient, using the temperature dependence reported by (Dunlop and Tully, 1993). A more detailed description of this method is described within instrument characterization (Section 3.4).

Atmos. Meas. Tech. Discuss., https://doi.org/10.5194/amt-2019-164
Manuscript under review for journal Atmos. Meas. Tech.
Discussion started: 10 May 2019

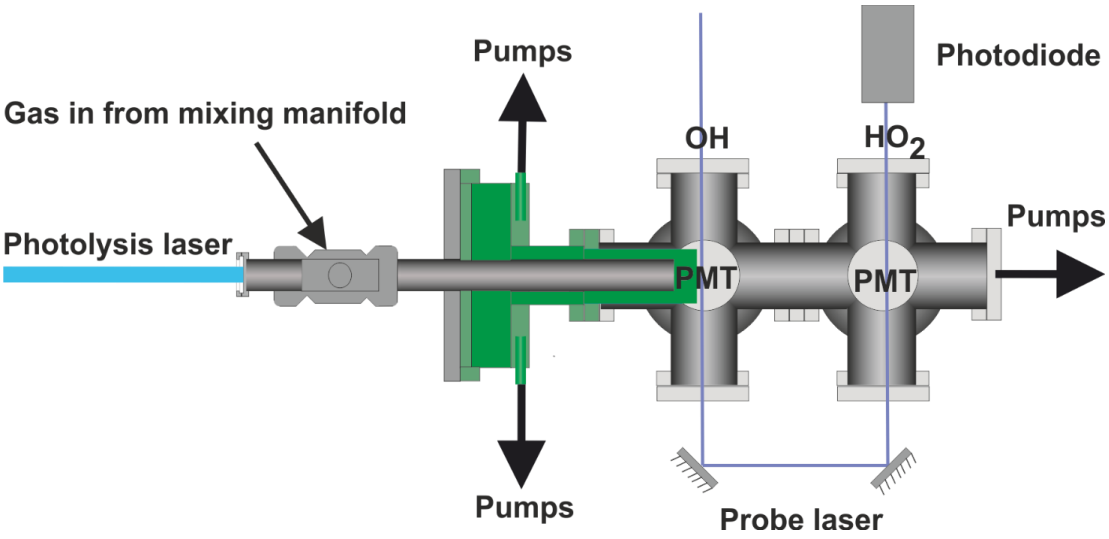

Figure 1. Schematic plan of the apparatus.

The photolysis of the OH precursor, H_2O_2, at 248 nm (Lambda Physik, Compex 200 operated using KrF) or 266 nm (frequency quadrupled Nd-YAG output, Quantel, Q-smart 850) initiated the chemistry.

$$H_2O_2 + h\nu \rightarrow 2OH \qquad \text{(R4)}$$

Hydrogen peroxide was used as the OH precursor for all experiments where HO_2 detection was performed, because it also acts as an internal calibrant to relate OH and HO_2, via reaction R5:

$$\mathbf{OH} + H_2O_2 \rightarrow H_2O + \mathbf{HO_2} \qquad \text{(R5)}$$

However, in general, other OH precursors can be used. The OH precursor was maintained at low concentrations ($1 \times 10^{14} – 1 \times 10^{15}$ molecule cm^{-3}) to minimise errors associated with assigning pseudo-first-order kinetics for the loss of OH, and to reduce radical-radical reactions. Maintaining a low radical precursor concentration had the additional advantage of minimising attenuation of the photolysis beam, ensuring consistency in the initial radical concentrations generated along the length of the high-pressure cell. Initial OH concentrations were in the range $2 \times 10^{11} – 5 \times 10^{13}$ molecule cm^{-3}.

Atmos. Meas. Tech. Discuss., https://doi.org/10.5194/amt-2019-164
Manuscript under review for journal Atmos. Meas. Tech.
Discussion started: 10 May 2019

A pinhole (diameter < 0.15 mm) at the end of the high-pressure reactor couples the reactor to the low-pressure (0.3 – 5 Torr) detection cell. Details on OH detection can be found in Stone et al. (2016). The accuracy of the instrument for OH measurement has recently been verified by measurements of the rate coefficient of the reaction of OH with isoprene (Medeiros et al., 2018) which are in excellent agreement with the literature. A more detailed schematic for the low-pressure detection cell is shown in Figure 2.

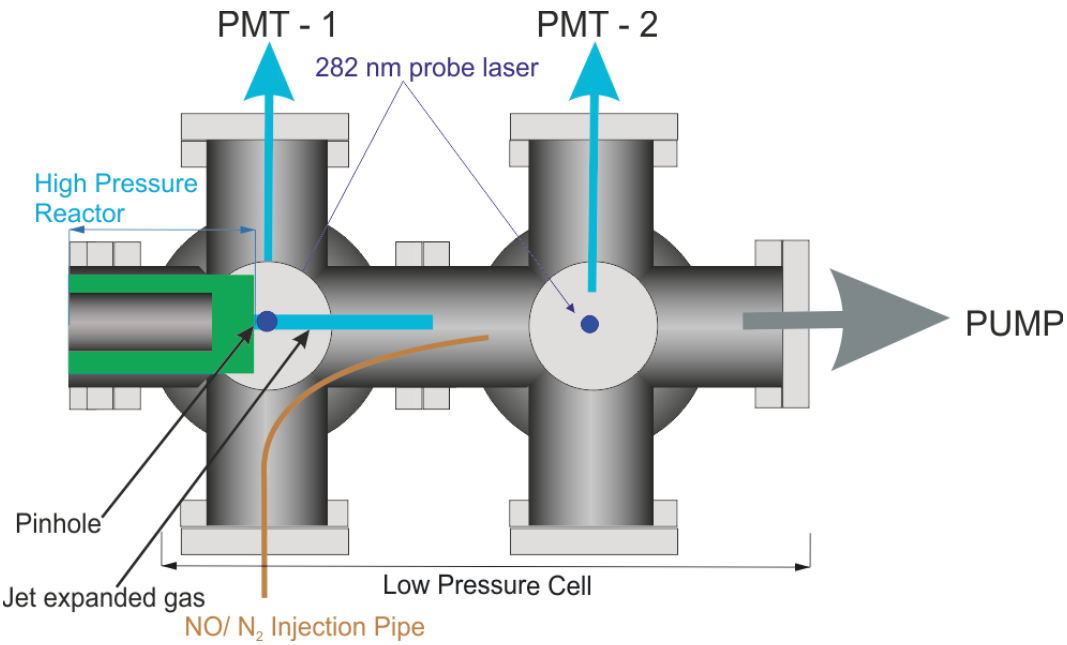

Figure 2. Detailed schematic elevation of the low-pressure detection region of the reactor. The blue line represents the jet expanded gas; the jet breaks down after approximately 2 cm. NO was injected through a 1.5 mm id stainless steel tube after the breakdown of the jet.

In the first low pressure detection cell, the OH was probed within the jet expanded gas, close to pinhole (<5 mm), perpendicular to the gas flow. The OH was detected by off-resonance laser induced fluorescence (LIF) at 308 nm following excitation with 282 nm light ($A^2\Sigma$ (v′ = 1) ← $X^2\Pi$(v″ = 0),Q_{11}). The 282 nm light was the frequency doubled output of a dye laser ((Rhodamine 6 G, Spectron) pumped at 532 nm by a Nd:YAG laser (Spectron), or (Rhodamine 6 G, Continuum) pumped by a Nd-YAG laser (Quantel, Q-smart 850)). Measuring the off-resonance

fluorescence allowed the use of a filter (308 ± 5 nm, Barr Associates) before the photomultiplier (Perkin-Elmer C1943P) to remove scattered light and improved the signal to noise ratio.

A delay generator (BNC DG535) was used to vary the delay between the photolysis and probe laser, facilitating generation of time profiles of the OH concentration. The traces were scanned through multiple times (5 – 20) and the signal at each time point was averaged, giving high precision OH loss traces. An example OH trace from the first detection cell for reaction R5 is presented in Figure 3. As reactions were carried out under pseudo first order conditions ([OH] << [substrate]), the time dependence of the OH LIF signal, I_f, (proportional to the [OH]) was given by:

$$I_{f,t} = I_{f,0} e^{-k_{\mathrm{OH}} t}$$

where $k_{\mathrm{OH}} = k_5[H_2O_2]$. In Figure 3 two traces are presented from the first, OH, detection axis, these two traces were taken in consecutive experiments with a constant $[H_2O_2]$ where the first trace ($k_{\mathrm{OH,1st}}$ = (2351 ± 22) s^{-1}) was taken where N_2 was flowed into the low pressure region, the second trace ($k_{\mathrm{OH,1st}}$ = (2389 ± 18) s^{-1}) was taken when this flow had been switched to NO to allow HO_2 detection in the second detection cell, errors are given as 2 σ. The similarity of the OH decay traces when either N_2 or NO was injected shows that there was no back streaming of NO in the low-pressure cell and hence no HO_2 conversion at the first detection axis.

HO_2 radicals were monitored by the chemical transformation of HO_2 to OH via reaction with NO (R3) in the low-pressure cell. Following the breakdown of the jet, after the Mach disk (>2 cm beyond the pinhole), a small flow (5 sccm) of NO or N_2 was introduced into the low-pressure cell via a 1.5 mm i.d. stainless steel pipe (for a typical 0.5 Torr pressure in the FAGE cell the NO concentration was 5.5×10^{13} molecule cm^{-3}). After passing through the first detection cell, the probe beam was redirected through the second low-pressure detection cell downstream of the NO pipe allowing for the measurement of the OH concentration by LIF in the same manner as in the first cell.

Atmos. Meas. Tech. Discuss., https://doi.org/10.5194/amt-2019-164
Manuscript under review for journal Atmos. Meas. Tech.
Discussion started: 10 May 2019

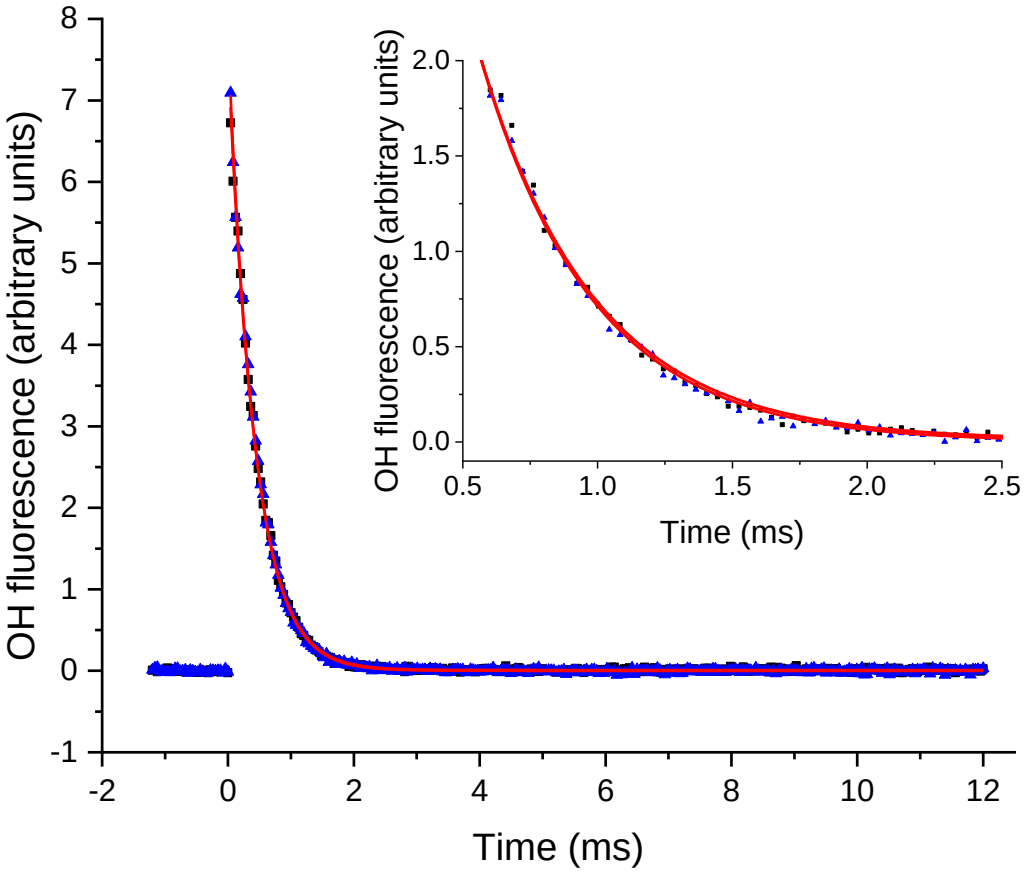

Figure 3. An example of the OH signal (blue triangles) collected at the first detection axis for the reaction of OH with H_2O_2 ($[H_2O_2] \approx 1.4 \times 10^{15}$ molecule cm^{-3}, with a flow of N_2 into the low-pressure cell, with black squares representing the subsequent trace taken with a flow of NO. The red lines represent the non-linear least squares fits to an exponential decay ($k_{OH,1st}$ = (2351± 22) s^{-1} and $k_{OH,1st}$ = (2389 ± 18) s^{-1}), 2 σ errors.

By switching between a flow of N_2 and NO, through the pipe, traces for OH loss and HO_2 formation could be elucidated, examples of which are shown in Figure 4. Subtraction of the two OH traces in Figure 4, (upper, red trace is with NO injection and the signal corresponds to reactant OH and OH produced from the titration of HO_2 to OH, lower, blue trace with N_2 injection is reactant OH only) gave a resultant signal associated with HO_2 production in the high-pressure reactor, shown the pink trace in Figure 4. The signal from the first PMT allowed for correction of

Atmos. Meas. Tech. Discuss., https://doi.org/10.5194/amt-2019-164
Manuscript under review for journal Atmos. Meas. Tech.
Discussion started: 10 May 2019

the signal heights at the second PMT for changes in the probe laser power or wavelength, any variations in laser power or wavelength affect the absolute signal retrieved from both PMTs; however, the relative signals retrieved from the PMTs remain consistent.

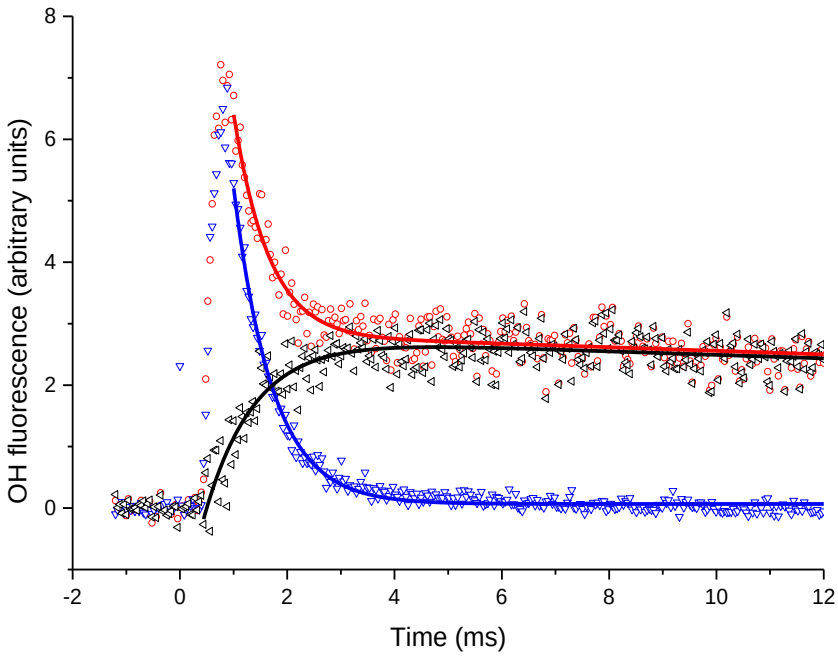

Figure 4. Examples of OH fluorescence traces collected at the second detection axis under the same conditions for Figure 3. The blue triangles are where N_2 has been injected through the pipe, i.e. no HO_2 to OH conversion. The OH signal profile differs from that in Figure 3, with $k_{OH,2nd}$ = (1390 ± 44) s^{-1} (2 σ errors), additionally, there is a time-delay to peak OH, representing the transport time (primarily the time taken to travel from the breakdown of the jet to the second detection axis). The red circles are the OH signal obtained with NO injection. At short times the signal is dominated by reactant OH, but at times greater than 2 ms, the signal is dominated by OH titrated from the HO_2 product. The resultant OH trace associated with HO_2 formation in the high-pressure cell obtained by subtracting the two OH traces, obtained with either NO or N_2 injection prior to the second detection axis, shown as black triangles, a biexponential growth and decay fit, black curve, gave a formation rate coefficient, $k_{HO2,2nd}$ = (1080 ± 150) s^{-1} (2 σ error).

Fits to the HO_2 formation traces and OH loss traces from the second cell generated kinetic parameters which differed from the accurate parameters collected at the first detection axis, $k_{OH,2nd}$

= (1390 ± 44) s^{-1} and $k_{HO2,2nd}$ = (1080 ± 150) s^{-1} where the accurate loss parameters from the first cell were $k_{OH,1st}$ = (2389 ± 18) s^{-1}, 2 σ errors. This difference was the result of transport effects. By comparison of the loss and formation parameters derived for OH + H_2O_2, for the first and second detection cells, HO_2 formation rates could be assigned from a calibration plot (Figure 7).

Neither of the OH determinations in the two detection axes provide absolute measurements of radical concentrations. Each detection axis could be calibrated as for chamber measurements, but for our purposes a calibration reaction linking photolytically produced OH and HO_2 removes many sources of error compared to an absolute calibration. The reaction of OH with the radical precursor H_2O_2 which directly forms HO_2 with a 100 percent yield was used for calibration.

$$\mathbf{OH} + H_2O_2 \rightarrow H_2O + \mathbf{HO_2} \qquad \text{(R5)}$$

For reactions carried out where a reagent was added in addition to the H_2O_2, the resulting ratios can be compared with those from the calibration reaction to allow assignment of an observed HO_2 yield. To assign the HO_2 yield from the test reaction required accounting for secondary HO_2 production in the high-pressure reactor, from OH + H_2O_2 and photolysis processes. From the known rate coefficients, it was possible to calculate the fraction of OH reacting with the H_2O_2 and hence the expected contribution to the HO_2 signal. Photolytic production of HO_2 was accounted for by measuring the observed HO_2 signal in the absence of any H_2O_2.

In a typical experiment, the reaction of OH and H_2O_2 would be carried out four times, twice in the absence of NO and twice with the addition of NO to calibrate the instrument. Exponential fits to the OH decay as monitored in the first cell determine the peak OH signal. The OH signals at the second detector recorded with only N_2 addition (reagent OH reaching the second detector) and subtracted from the signal with NO added (reagent OH and HO_2) to give the net HO_2 signal. This profile was fitted to, a biexponential growth and decay function, to extract the peak HO_2 signal for that set of conditions. Combinations of traces were then used to obtain an averaged value (and uncertainty) of the signal on the first PMT (OH) to the net HO_2 signal at the second PMT for this calibration reaction where OH reactant and HO_2 product have a 1:1 relationship. The same process was then performed in the presence of the compound of study. The removal pseudo-first-order rate coefficient with H_2O_2 and the reagent of study ($k'_{OH,1st}$ = $k_{OH+H2O2}[H_2O_2]$ + $k_{OH+TEST}$[TEST]) was compared to the removal pseudo-first-order rate coefficient with only H_2O_2

($k'_{OH,1st} = k_{OH+H2O2}[H_2O_2]$) to assign what fraction of the OH reacted with the H_2O_2 precursor and hence the resulting contribution to the observed HO_2. Comparison of the remaining peak ratio to the ratio from the H_2O_2 and OH calibration experiment provided the experimentally derived HO_2 yield for reaction of OH and the reagent of study.

Branching ratios to direct HO_2 formation could be assigned with an accuracy of ~10 %, the limitations to this were signal to noise effects, where improved signal to noise could be achieved by increasing the precursor concentration and photolysis energy. However, this was limited by the need to ensure pseudo-first-order conditions were maintained and to minimize radical-radical processes. Ensuring the dominant reaction was between OH and the reagent of study, whilst still being able to accurately measure the initial OH conditions, provided a limit to the maximum removal rates achievable ($k_{OH,1st} < 30{,}000\ s^{-1}$).

3 Instrument Characterization

Many reactions of atmospheric and combustion interest are studied in the presence of oxygen leading to the generation of peroxy radicals (RO_2). For certain RO_2 there is a potential to generate OH and HO_2 on a fast timescale and therefore three well known reactions were chosen to characterize the instrument, OH and ethane, OH and ethylene, and OH and methanol.

$$OH + C_2H_6 \rightarrow H_2O + C_2H_5 \quad \text{(R6)}$$

$$OH + C_2H_4 \rightarrow HOC_2H_4 \quad \text{(R7)}$$

$$OH + CH_3OH \rightarrow H_2O + CH_2OH,\ CH_2OH + O_2 \rightarrow HO_2 + HCHO \text{ (fast)} \quad \text{(R8a, R9)}$$

$$OH + CH_3OH \rightarrow H_2O + CH_3O,\ CH_3O + O_2 \rightarrow HO_2 + HCHO \text{ (slow)} \quad \text{(R8b, R10)}$$

OH and ethane (R6) gives an assessment of any false yields generated from RO_2 and NO from prototypical alkyl RO_2 species that will be formed from many atmospherically relevant reactions. Ethylene and OH (R7) forms a hydroxy alkyl peroxy radical, the typical RO_2 species known to create interferences in FAGE HO_2 detection systems (Fuchs et al., 2011;Hard et al., 1984;Whalley et al., 2013). Minimizing and understanding the HO_2 yield from this reaction allowed for limits to the selectivity of the instrument to be known. The reaction of OH with methanol is a well

understood reaction; the two isomeric radical products react with oxygen on differing timescales to generate HO_2. Complete conversion of both isomers should yield 100 % HO_2.

As discussed in the experimental section, transport effects after the breakup of the sampling jet mean that rate coefficients measured in the second cell $k_{X,2nd}$ (X = OH or HO_2) differ from each other (transport effects scale with mass) and from those made in the first detection axis ($k_{OH,1st}$). Pseudo-first-order rate coefficients from the two detection axes were compared to ascertain whether measurements in the second detection axes can be used to make quantitative kinetic measurements.

Finally, the layout of the apparatus makes it hard to accurately measure the temperature at which the reaction occurs; for reactions occurring on a millisecond timescale, the relevant reaction distance from the sampling pinhole is approximately 0.05 - 0.5 mm. Compared to a conventional slow flow laser flash photolysis/laser induced fluorescence apparatus, where the reaction volume is the overlap of the perpendicular photolysis and probe laser beams, it is hard to accurately position the thermocouple and additionally, any thermocouple located close to the sampling pinhole may affect the flow into the low pressure system. In addition to the difficulties in correctly siting a thermocouple, there are additional errors (flow, conduction and radiative) that derive from measuring the temperature of a flowing gas with a thermocouple. We have therefore performed additional experiments to determine the temperature based on the well characterized and temperature sensitive reaction of OH and methane.

3.1 Interference by RO_2 species

Selectivity in measuring HO_2 concentrations plays an important role in the viability of detection methods for monitoring reactions important for atmospheric chemistry. At high pressures, the reaction of NO with many atmospherically relevant RO_2 species in the presence of oxygen induces HO_2 formation. By performing the titration in the low-pressure cell with the NO + HO_2 reaction under 'starved NO' conditions minimized this effect. This premise was validated by measuring the OH + ethane and OH + ethylene HO_2 yields under high oxygen conditions. In our system the typical oxygen concentrations in the high pressure reactor were varied between 1×10^{16} and 5×10^{17} molecule cm^{-3} which led to concentrations in the low pressure cell of 3×10^{12} to 2×10^{15} molecule cm^{-3}.

The reaction of OH + ethane (R6) under high oxygen conditions permits the rapid formation of the ethylperoxy radical, which is an RO_2 radical that has a typical slow, NO propagated, route to HO_2 formation (R11 – R12).

$CH_3CH_2O_2 + NO \rightarrow CH_3CH_2O + NO_2$ (R11)

($k_{11,\,298\,K} = 8.70 \times 10^{-12}$ cm^3 molecule^{-1} s^{-1}) (Atkinson et al., 2006)

$CH_3CH_2O + O_2 \rightarrow CH_3CHO + HO_2$ (R12)

($k_{12,\,298\,K} = 9.48 \times 10^{-15}$ cm^3 molecule^{-1} s^{-1}) (Atkinson et al., 2006)

Under a variety of NO flows the apparent HO_2 yield for the OH + C_2H_6 system was 3 ± 6 %, which indicates that for most reactions carried out in our system, chemical transformation by reaction with NO, was sensitive to HO_2 rather than RO_2 species, where the RO_2 radical was the product of O_2 addition to a simple alkyl radical.

The reaction of ethylene and OH (R7) in the presence of oxygen forms the hydroxyethylperoxy radical ($HOCH_2CH_2O_2$), and reaction of the $HOCH_2CH_2O_2$ with NO in the presence of O_2 provides a route for the prompt regeneration of OH. For this reaction, an apparent HO_2 yield of 100 ± 15 % was observed; however, by varying the concentration of NO added to low pressure cell (between 5×10^{13} and 5×10^{14} molecule cm^{-3}), the formation rate of OH was reduced minimizing the apparent yield observed (<70 %) and slowing the observed rate of OH regeneration (<1000 s^{-1}).

$HOCH_2CH_2O_2 + NO \rightarrow HOCH_2CH_2O + NO_2$ (R13)

($k_{13,\,298\,K} = 9.00 \times 10^{-12}$ cm^3 molecule^{-1} s^{-1}) (Atkinson et al., 2006)

$HOCH_2CH_2O \rightarrow CH_2O + HOCH_2$ (R14)

($k_{14,\,298\,K} = 1.3 \times 10^{5}$ s^{-1}) (Orlando et al., 1998)

$CH_2OH + O_2 \rightarrow CH_2O + HO_2$ (R9)

($k_{9,\,298\,K} = 9.60 \times 10^{-12}$ cm^3 molecule^{-1} s^{-1}) (Atkinson et al., 2006)

For test reagents which can generate radicals similar to hydroxyethylperoxy, our instrument will detect both HO_2 and RO_2 with some selectivity to HO_2.

Atmos. Meas. Tech. Discuss., https://doi.org/10.5194/amt-2019-164
Manuscript under review for journal Atmos. Meas. Tech.
Discussion started: 10 May 2019

3.2 OH + methanol

To verify the accuracy of the method for determining HO_2 yields the reaction of OH and methanol (R8) was examined. The branching ratio for the α abstraction to yield CH_2OH (R8a) reported by the IUPAC evaluation and based on the experimental data of McCaulley et al. (1989), is α = (85 ± 8)% at room temperature with the methoxy yield as (15 ± 8)%. Reaction R8 was studied at room temperature with the reaction being initiated by the photolysis of H_2O_2 at 248 nm. In the presence of low concentrations of oxygen (< 1 × 10^{16} molecule cm^{-3}), the α abstraction still leads to prompt formation of HO_2 via R9, but R10, $CH_3O + O_2$, occurs on a much longer timescale and is not observed under these conditions. The observed HO_2 yield, (87 ± 10)% (first row of Table 1) gives the fraction of reaction R8 forming CH_2OH and the value is consistent with the IUPAC evaluation.

Table 1. HO_2 yields from the reaction of OH with CH_3OH with varying [O_2] carried out 295 K. Errors given as 2 σ.

[O_2]/ molecule cm^{-3}	HO_2 Yield (%)				Average HO_2 Yield (%)
	Expt 1	Expt 2	Expt 3	Expt 4	
<1 × 10^{16}	90	89	79	88	(87 ± 10)
>2 × 10^{18}	93	94	100	99	(97 ± 6)

When higher concentrations of oxygen are used, the timescale for HO_2 production from reaction R10 decreases and now both abstraction channels lead to HO_2 detection in our apparatus. The resulting observed yield (second row of Table 1) is consistent with 100% conversion of OH to HO_2. The reproduction of the literature HO_2 yields from the reaction of OH with methanol under varying [O_2] demonstrates that the instrument can accurately measure HO_2 yields with good precision. It has additionally been demonstrated that the instrument had sufficient accuracy and precision to assign the branching ratios for differing abstraction channels when it was possible to separate the channels by the timescale for HO_2 generation.

3.3 Assessment of transport effects on observed kinetics

Due to the differing conditions in the two detection regions, the kinetics observed at the first detection axis, where OH LIF was performed in the jet-expanded gas, and in the second detection region, where LIF is performed 15 cm downstream from the pinhole after the breakdown of the jetting gas, will be treated separately. For validating the accuracy of the OH kinetics in the first cell, the reactions of OH and methane (CH_4) (Dunlop and Tully, 1993), OH and ethylene (C_2H_4) (Atkinson et al., 1982;Tully, 1983) were studied. The high accuracy and precision of this system for measuring OH kinetics has further been demonstrated in a recent publication on the reaction of OH and isoprene (C_5H_8) (Medeiros et al., 2018).

$$OH + CH_4 \rightarrow H_2O + CH_3 \quad \text{(R15)}$$

$$OH + C_2H_4 \rightarrow HOC_2H_4 \quad \text{(R7)}$$

$$OH + C_5H_8 \rightarrow HOC_5H_8 \quad \text{(R16)}$$

When these reactions were carried out at room temperature the expected bimolecular rate coefficients could be reproducibly accurately measured for observed rate coefficients less than 150,000 s^{-1}.

Studies on the reaction of OH and ethylene at room temperature and 2.2 bar, shown in Figure 5, gave a value of $k_7 = (8.33 \pm 0.16) \times 10^{-12}$ cm^3 $molecule^{-1}$ s^{-1} (2σ errors) which matched well with literature high pressure limits for OH and ethylene; where a direct pulsed laser photolysis laser induced fluorescence study by Tully (1983) gave $k_7 = (8.47 \pm 0.24) \times 10^{-12}$ cm^3 $molecule^{-1}$ s^{-1}, and a relative rate study by Atkinson et al. (1982) found $k_7 = (8.11 \pm 0.37) \times 10^{-12}$ cm^3 $molecule^{-1}$ s^{-1}. However, for pseudo-first order rate coefficients above ~150000 s^{-1}, there was no longer a linear dependence of the rate coefficient with reagent concentration; transport effects are becoming significant even for OH detection in the jetting region.

Atmos. Meas. Tech. Discuss., https://doi.org/10.5194/amt-2019-164
Manuscript under review for journal Atmos. Meas. Tech.
Discussion started: 10 May 2019

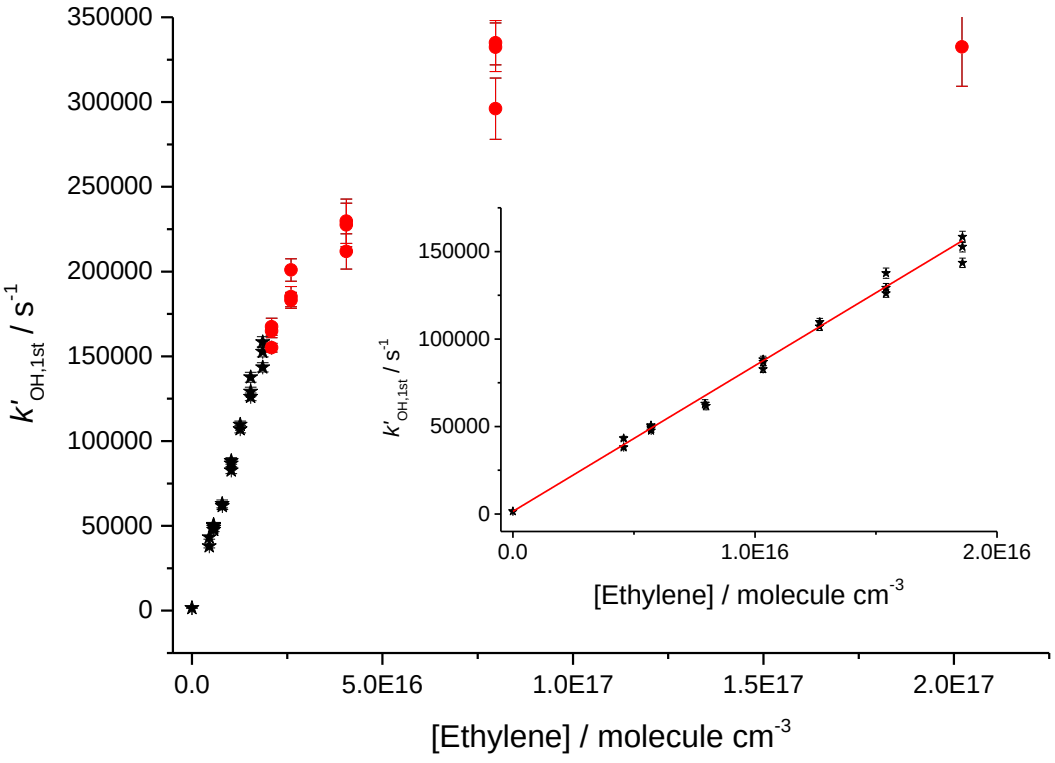

Figure 5. Bimolecular plot of the pseudo-first-order rate coefficient at the first detector, $k'_{OH,1st}$, vs ethylene concentration. The figure demonstrates a linear relationship below ~150,000 s^{-1} (see inset for detail in linear region) but with increasing curvature, due to transport effects at higher values of $k'_{OH,1st}$. Black stars symbolize where $k'_{OH,1st}$ was linear with [C_2H_4], red circles where $k'_{OH,1st}$ showed greater than 5% deviation from linearity.

The OH traces detected in the second cell deviated from those observed from the first cell, as shown in Figures 3 and 4. There is understandably an increased time delay from time zero (the photolysis laser pulse) to arrival of OH radicals at the second detection axis due to the increased distance travelled after sampling (> 150 mm versus < 5 mm). Additionally, the arrival of OH to the second axis is spread out further in time due to transport issues relating to non-linear flow conditions at the breakdown of the jet, and the arrival of the OH being affected by its velocity distribution (Moore and Carr, 1977;Taatjes, 2007;Baeza-Romero et al., 2012). Figure 6 shows a plot of observed OH rate coefficient from the first detection axis ($k_{OH,1st}$) against observed rate coefficient from the second axis ($k_{OH,2nd}$). For values of k_{OH} below 2500 s^{-1} it was possible to

Atmos. Meas. Tech. Discuss., https://doi.org/10.5194/amt-2019-164
Manuscript under review for journal Atmos. Meas. Tech.
Discussion started: 10 May 2019

accurately assign an expected OH removal rate for reactions observed in the second cell ($k_{OH,2nd}$) given the observed OH kinetics at the first detection axis ($k_{OH,1st}$). This is useful to compare the kinetics of OH removal and HO_2 production.

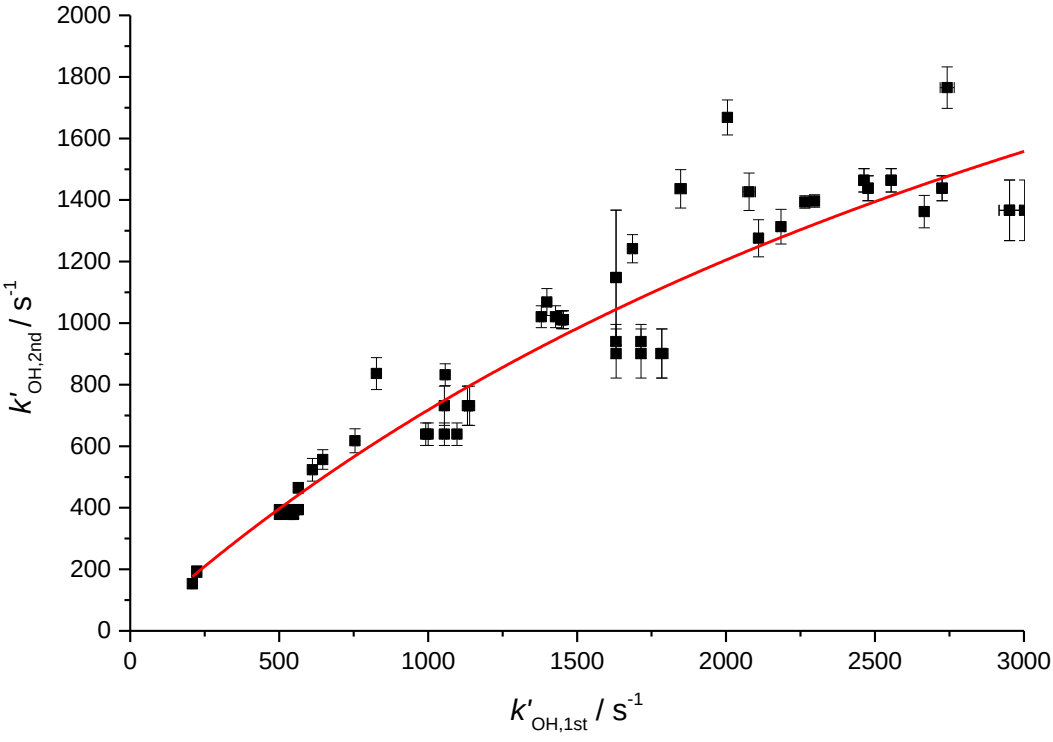

Figure 6. Relationship between the observed rate coefficient observed in the first cell ($k_{OH,1st}$) and the observed OH removal rate in the second cell ($k_{OH,2nd}$). The difference is non-linear but a simple fit to this could be used to assign removal rates to traces observed in the second cell below 2,500 s^{-1}. The red line is the simplified fit of the form, $y = A * (1 - e^{-b*x})$, where A was some limit value above which no increase in measured rate coefficient would be observed.

As the observed kinetics in the second cell are significantly affected by the velocity distribution of the species being detected, there is again a deviation between the observed kinetics expected from the measurement of the OH radicals loss and the kinetics for HO_2 formation due to the differing masses of OH and HO_2. Figure 7 shows the pseudo-first order rate coefficients for OH removal ($k'_{OH,2nd}$) and HO_2 production ($k'_{HO2,2nd}$) determined at the second detection axis, plotted against the OH removal at the first detection axis. The two fits to the data shown in Figure

Atmos. Meas. Tech. Discuss., https://doi.org/10.5194/amt-2019-164
Manuscript under review for journal Atmos. Meas. Tech.
Discussion started: 10 May 2019

7 had a ratio of gradients concordant with the root of the masses for HO_2 and OH, 0.60 ± 0.14 versus the expected relationship of 0.73. As with Figure 6, it is possible to establish a calibration graph that relates the kinetics of HO_2 production at the second detection axis with the primary kinetics taking place in the high pressure reactor. This means that the timescale over which the HO_2 yield was observed could be assigned and therefore it is possible to attribute HO_2 yields to fast processes, intramolecular RO_2 decompositions or R + O_2 reactions, or to slower radical-radical reactions.

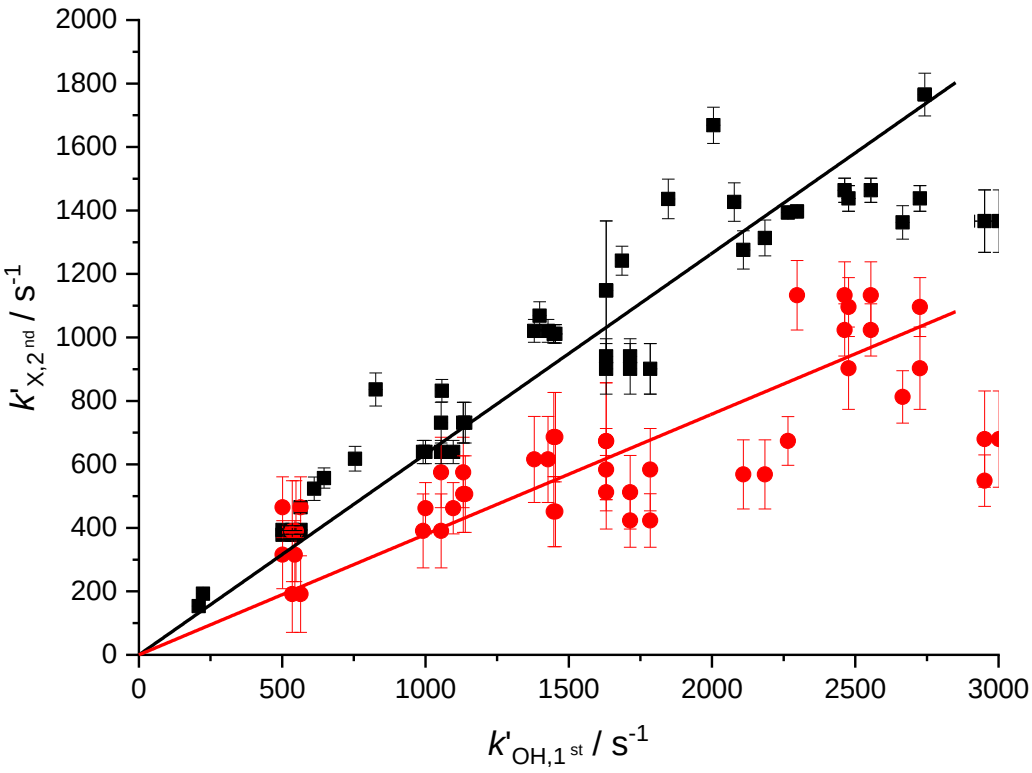

Figure 7. Relationship between the pseudo-first-order rate coefficient for OH loss observed in the first cell ($k'_{OH,1st}$) and the observed rate coefficients in the second cell ($k'_{X,2nd}$ where X = OH or HO_2) a non-linear fit can be used to assign removal rates and HO_2 formation rates to traces observed in the second cell below 2,500 s^{-1}.

3.4 Temperature corrections

It is difficult to know the exact temperature at the pinhole as introducing a thermocouple close to the region will affect the flows and cannot be used in routine operation. A translatable thermocouple was passed along the axis of the high-pressure reactor over a variety of temperatures and showed that the temperature of the gas at the pinhole varies with axial location. In addition, radial profiles showed that in our system there was insufficient heating length to achieve uniform radial heating of the laminar gas. From the axial measurements it was observed that slower flow rates (< 5 SLM) allowed for reduced axial temperature gradients. However, these measurements showed that the only manner to achieve an even thermal profile would be a static cell.

A permanently seated thermocouple was placed perpendicularly to the flow, close to the sampling region, measurements from this thermocouple were then compared with temperature assignments from the reaction of OH and methane using the temperature dependence assigned by Dunlop and Tully (1993). This was performed over a range of heater settings and flows to allow for temperature assignment. This method was also applied to a standard low-pressure cell where the flows can be reduced to slow enough flows that thermocouple measurements could accurately define the temperature to verify the method. Additionally, the well-determined OH + ethylene adduct formation equilibrium was measured over a range of temperatures to provide an additional verification of the temperature assignment.

The method to assign a temperature from the reaction of OH and methane used the pseudo-first order rate coefficients ($k'_{OH,1st}$) measured at the first detection axis over a range of added methane flows. An estimate of the temperature was made from the thermocouple measurement, this estimated temperature was used, along with the pressure in the reactor, to calculate the added methane concentration. Comparing the predicted pseudo-first-order rate coefficient that this estimated concertation provided using the literature value of k_{OH+CH4} (Dunlop and Tully, 1993) to the measured rate coefficient produced a difference for each point. The estimated temperature was then iteratively changed to minimize the difference between estimated and measured rate coefficients. For this minimum value, the difference between thermocouple measurement and actual temperature was tabulated against the voltage setting for the heater. A parameterization of voltage versus temperature difference was used to estimate the temperature of the reactor for experiments where no OH and methane measurements were performed and has been shown to

Atmos. Meas. Tech. Discuss., https://doi.org/10.5194/amt-2019-164
Manuscript under review for journal Atmos. Meas. Tech.
Discussion started: 10 May 2019

reliably predict the temperature of the reactor within 7 K when measurements have been made subsequently.

To assess the axial temperature gradients in the gas sampled through the pinhole over the timescales of reactions measured, OH and methane rate coefficients were measured using photolysis of water at 193 nm as a source of OH. Using water photolysis allowed for low removal rates of OH by precursor and assignment of OH and methane over a range of pseudo-first-order rate coefficients ($k'_{OH,1st}$) 100 – 40000 s^{-1} as shown in Figure 8. This was performed at two temperatures (505, 680 K), and the slope of observed OH removal rate coefficients against concentration of methane appeared linear over the full range for both temperatures, thus verifying that over the distances sampled within experimental timeframes there is a minimal temperature gradient.

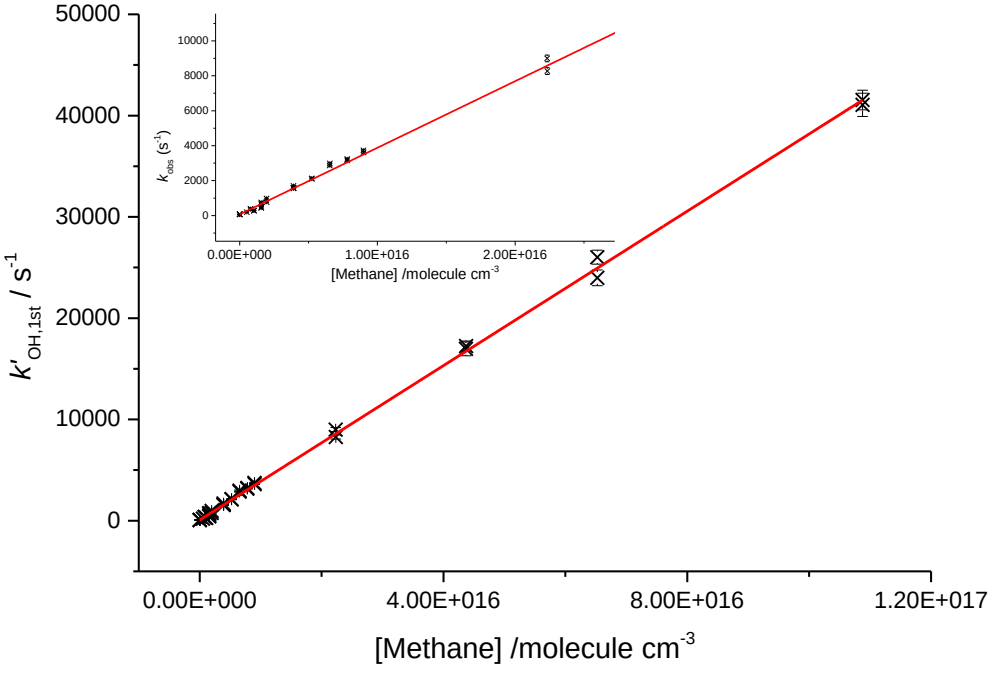

Figure 8. Bimolecular plot for the reaction of OH and methane at 680 K, 1760 Torr using 193 nm photolysis of water as an OH precursor. Here the inset shows that even at removal rates < 1000 s^{-1} the plot is still linear, indicating that within the measured experimental timescales there is little deviation in temperature.

Atmos. Meas. Tech. Discuss., https://doi.org/10.5194/amt-2019-164
Manuscript under review for journal Atmos. Meas. Tech.
Discussion started: 10 May 2019

4 Determination of Site Specific Rate Coefficients for the Reaction of OH with n-butanol

The branching ratios for the sites of OH attack on n-butanol, as presented in Scheme 2, are of significance to the modelling of the ignition delay times for n-butanol (Agbro et al., 2017). Abstractions at the α and OH positions are chain terminating reactions at low temperatures due to the formation of the relatively inert HO_2 radical, and abstraction at the β site leads to chain propagation, through OH recycling. The new instrument permitted determination of the attack at the α and β sites; attack at the α site leads to prompt HO_2 formation in the presence of O_2; at elevated temperatures biexponential fits to non-single exponential OH loss traces in the absence of O_2 (due to decomposition of the β hydroxy radical to OH and iso-butene) allowed for attack at the β site to be measured.

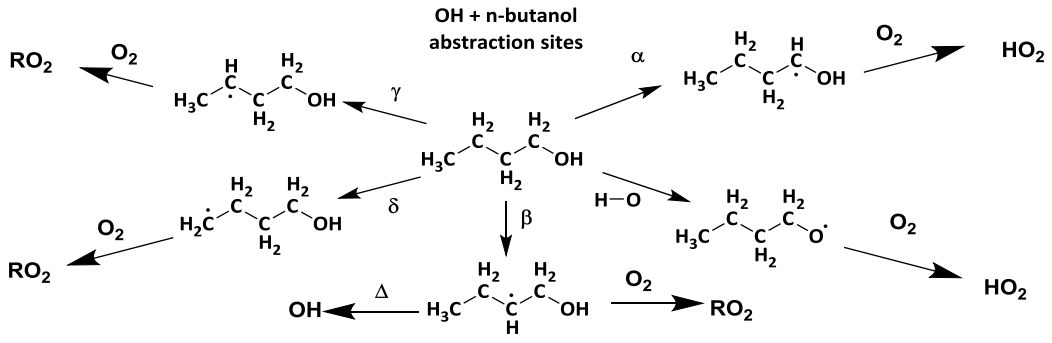

Scheme 2. The potential sites for OH abstractions in the oxidation of n-butanol. Of particular importance to low temperature combustion is the ratio of α to β branching fractions where α attack leads to chain inhibition and beta to chain propagation.

4.1 Room temperature OH kinetics

At room temperature under pseudo-first-order conditions ([OH] < 3 × 10^{12} molecule cm^{-3}, [n-butanol] > 1.5 × 10^{14} molecule cm^{-3}), the OH loss traces recovered from the first detection axis from the jet expanded gas corresponded closely with single exponential decays. These decays relate to the overall loss process for the reaction of OH with n-butanol:

$$OH + n\text{-}C_4H_9OH \rightarrow H_2O + \text{isomers of } C_4H_9O \qquad (R1)$$

Atmos. Meas. Tech. Discuss., https://doi.org/10.5194/amt-2019-164
Manuscript under review for journal Atmos. Meas. Tech.
Discussion started: 10 May 2019

The resulting rate coefficients were plotted against the concentration of butanol, in the presence of both low and high oxygen, as shown in Figure 9 (low oxygen < 5 × 10^{15} molecule cm^{-3}, high oxygen 1.2 × 10^{19} molecule cm^{-3}), where $k_{obs} = k_1 \times$ [butanol], giving a resultant bimolecular removal rate of $k_1 = (9.24 \pm 0.40) \times 10^{-12}$ cm^3 $molecule^{-1}$ s^{-1} under low oxygen conditions, and $k_1 = (9.23 \pm 0.15) \times 10^{-12}$ cm^3 $molecule^{-1}$ s^{-1} under high oxygen conditions.

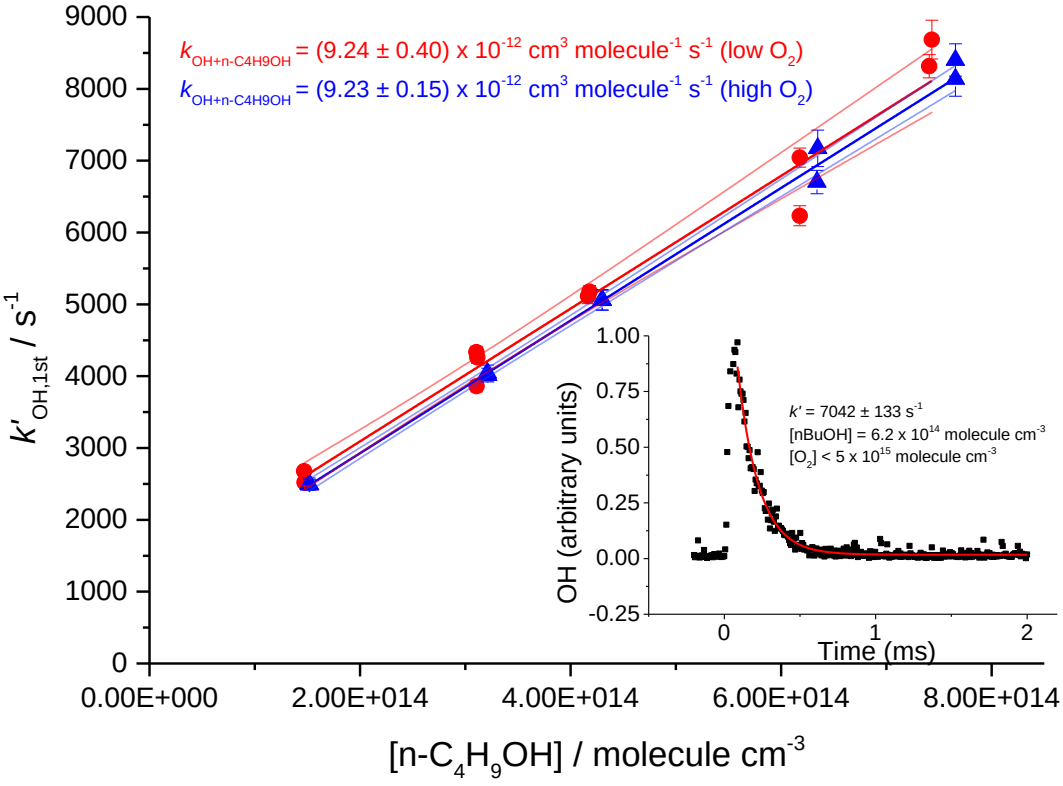

Figure 9. Plots $k'_{OH,1st}$ against the concentration of butanol, at two oxygen concentrations, < 5 × 10^{15} molecule cm^{-3} and 1.2 × 10^{19} molecule cm^{-3}. Bimolecular rate coefficients were taken from the slopes as (9.24 ± 0.40) × 10^{-12} cm^3 $molecule^{-1}$ s^{-1} under low oxygen conditions (red circles with 95 % confidence limits), and (9.23 ± 0.15) × 10^{-12} cm^3 $molecule^{-1}$ s^{-1} under high oxygen conditions (blue triangles with 95 % confidence limits). The inset shows a typical OH temporal profile at the first detection axis.

The good agreement between the measured rate coefficients with varying [O_2] verifies that, as expected under our experimental conditions at room temperature, the R radical formed from the β abstraction does not undergo fragmentation to OH and but-1-ene. The resultant combined data gives an overall 293 K bimolecular rate coefficient for OH and n-butanol of $k_1 = (9.24 \pm 0.21) \times$

10^{-12} cm^3 molecule^{-1} s^{-1}, which is in excellent agreement with the recent work of McGillen et al. (2013) of $k_{1,296}$ = (9.68 ± 0.75) × 10^{-12} cm^3 molecule^{-1} s^{-1}.

4.2 Room temperature HO_2 results

Experiments were carried out in high oxygen conditions (3 × 10^{17} – 1.2 × 10^{18} molecule cm^{-3}), at 296 – 303 K, and high pressures (1800 – 2000 Torr) of N_2 bath gas using photolysis of hydrogen peroxide at two different wavelengths (248 nm and 266 nm), and the resulting HO_2 yields are shown in Table 2. The resulting HO_2 yield was determined to be (58 ± 7) % at 266 nm, and (55 ± 12) % at 248 nm. As there is no significant variation in the yield with laser wavelength or power, we can treat the data in Table 2 as 12 independent estimates of the yield, giving an averaged HO_2 yield of 57% with a standard error (95%) of 6%. Therefore under the experimental conditions (pressure >1800 Torr, [O_2] > 3 × 10^{17} molecule cm^{-3}), the HO_2 yield, which originates from OH attack at the α abstraction site, was (57 ± 6) %, with a minor contribution from abstraction from the hydroxyl group. The yield assigned is in good agreement with McGillen et al. (2013) 57%, and Cavalli et al. (2002) 52 ± 7 %.

Table 2. HO_2 yields from experiments carried out at room temperature (293 – 298 K) with reaction initiated by photolysis of H_2O_2 at 248 nm and 266 nm.

Laser wavelength/nm	HO_2 Yield (%)							Average HO_2 Yield (%)
	Expt 1	Expt 2	Expt 3	Expt 4	Expt 5	Expt 6	Expt 7	
266	61 ± 7	54 ± 4	46 ± 5	56 ± 7	54 ± 7	67 ± 10	66 ± 6	58 ± 7
248	63 ± 2	68 ± 2	48 ± 5	52 ± 5	49 ± 5			55 ± 12

Experiments were carried out with photolysis at 266 nm and at a variety of laser energies at 248 nm, the yields remained consistent with photolysis wavelength and power. Varying the laser power did alter the profiles of the HO_2 traces recovered; the growth rates remained unaffected but the tails changed; decreasing laser power slowed the removal rate of HO_2 (from greater than 100 s^{-1} to under 10 s^{-1}) showing that radical-radical processes are the main source of HO_2 loss from the system. If radical-radical reactions were an important source of any observed HO_2 yield changing laser power would have altered the HO_2 yield and additionally the HO_2 growth kinetics.

Atmos. Meas. Tech. Discuss., https://doi.org/10.5194/amt-2019-164
Manuscript under review for journal Atmos. Meas. Tech.
Discussion started: 10 May 2019

4.3 Higher temperature – HO_2 yield and OH recycling

The R radical formed from abstraction at the β site ($CH_3CH_2CHCH_2OH$) can regenerate OH and form butene, Scheme 2, in the absence of added oxygen. This process was not observed at ambient temperatures (293 – 305 K) but at elevated temperatures, 616 K – 657 K, the OH loss observed at the first detection axis was no longer well described by a single exponential loss process, Figure 10. The non-exponential decays formed were due to OH being returned following decomposition of the β R radical. Biexponential fits to the recycling traces gave the fraction of OH returned (Medeiros et al. 2018), with an average β branching fraction of (23 ± 4)%, Table 3.

Table 3. OH recycling and HO_2 yields from experiments carried out under elevated temperatures (> 600 K) all experiments were carried out with photolysis at 248 nm.

Temperature (K)	Fraction of OH returned (%)	Observed HO_2 Yield (%)
616	24.2 ± 4.1	54 ± 4
622	24.4 ± 4.9	
636	25.7 ± 5.6	
657	18.1 ± 4.0	

The HO_2 yield measured at an elevated temperature (616 K), where OH recycling was also observed, was 54 ± 4 % (Table 3) which is within error of the value (57 ± 6 %) measured at room temperature (293 K), although it is not possible to partition the HO_2 yield between α and OH abstraction. Over the temperature range tested the branching ratio for OH attack at the α position is therefore also likely to remain unchanged. With the sum of the α and β sites contributing (78 ± 4)%, at 616 K, the remainder of the abstraction (~22%) occurs at the δ and γ sites. These results are in excellent agreement of the product study of Cavalli et al. (2002) which found (52 ± 7)% α from the butanal product yield and (23 ± 4) % β from the propanal yield using FTIR detection and the site specific analysis by McGillen et al. (57 % α and 26% β). The product study of Hurley et al. (2009) found 44 ± 4 % α and 19 ± 2 % β values which are lower than our experimental values but are within the combined error ranges. However, it should be noted that the β branching fraction of 23 ± 4 % measured in this study was obtained at elevated temperatures, 616 – 657 K.

Atmos. Meas. Tech. Discuss., https://doi.org/10.5194/amt-2019-164
Manuscript under review for journal Atmos. Meas. Tech.
Discussion started: 10 May 2019

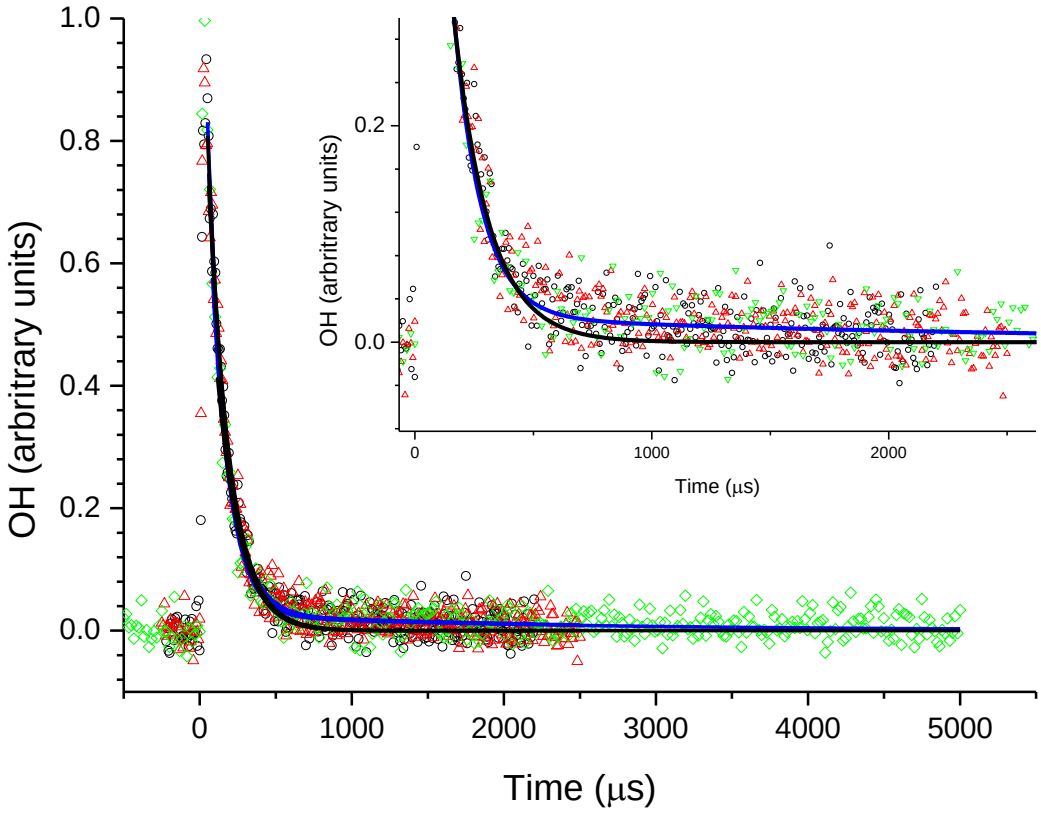

Figure 10. An example of the OH signal collected at the first detection axis for the reaction of OH with n-butanol ([nBuOH] ≈ 1.4 × 10^{15} molecule cm^{-3}, at 616 K The black line represents the least squares fits to an exponential decay ($k'_{1,1st}$ = (6780 ± 380) s^{-1}), with the blue line representing a bi-exponential fit ($k_{1,biexp,1st}$ = (8190 ± 180) s^{-1})).

5 Summary

The use of H_2O_2 as an OH precursor has been shown to provide a reliable method of internally characterizing our system for HO_2 yield detection. Interferences that could arise from using this precursor for HO_2 detection have been accounted for, and the presence of water that the H_2O_2 precursor introduces has no effect on the sensitivity of the LIF method, unlike IR absorption methods.

It has been demonstrated that this instrument can reliably assign HO_2 yields and simultaneously measure OH kinetics, even under conditions of high temperatures and high oxygen concentrations, which could be challenging for other detection systems. Such conditions are important for exploring key combustion chemistry reactions, and for converting slow atmospherically relevant processes to the microsecond timescales required to minimize secondary or heterogeneous chemistry.

By performing reactions under low NOx and low radical densities ($<1\times10^{13}$ molecule cm^{-3}), HO_2 yields formed on fast timescales (> 300 s^{-1}) can be assigned to direct HO_2 channels or reactions of alkyl (R) radicals with oxygen. Whilst some time-resolution is lost at the HO_2 detector, sufficient time-resolution is retained in order to separate varying sources of HO_2, for example the two channels leading to HO_2 production in the $OH/CH_3OH/O_2$ system (Section 3.2) or from unwanted secondary chemistry.

For particular reactions, illustrated in this paper by the study of OH with methanol and butanol in the presence of oxygen, the simultaneous measurement of OH kinetics and HO_2 yields can provide important site-specific information. In other systems, the onset of HO_2 formation could allow for the assignment of new channels becoming important within complex mechanism, potentially allowing for verifying the onset of OOQOOH chemistry within OH regeneration processes.

6 Acknowledgements

A studentship from NERC for T.H. Speak is gratefully acknowledged.

7 Author Contributions

THS undertook most of the experimental measurements and contributed to the first draft of the manuscript. DS provided input into experimental design and analysis of transport effects. MAB and PWS lead the project and completed the manuscript.

8 Competing Interests

The authors declare that they have no conflicts of interest.

9 References

Agbro, E., Tomlin, A. S., Lawes, M., Park, S., and Sarathy, S. M.: The influence of n-butanol blending on the ignition delay times of gasoline and its surrogates at high pressures, Fuel, 187, 211-219, 10.1016/j.fuel.201609.052, 2017.

Assaf, E., Liu, L., Schoemaecker, C., and Fittschen, C.: Absorption spectrum and absorption cross sections of the $2v_1$ band of HO_2 between 20 and 760 Torr air in the range 6636 and 6639 cm^{-1}, J. Quant. Spectrosc. Radiat. Transfer, 211, 107-114, 10.1016/j.jqsrt.2018.02.035, 2018.

Atkinson, R., Aschmann, S. M., Winer, A. M., and Pitts, J. N.: Rate constants for the reaction of OH radicals with a series of alkanes and alkenes at 299 +/- 2 K, Int. J. Chem. Kinet., 14, 507-516, 10.1002/kin.550140508, 1982.

Atkinson, R., Baulch, D. L., Cox, R. A., Crowley, J. N., Hampson, R. F., Hynes, R. G., Jenkin, M. E., Rossi, M. J., and Troe, J.: Evaluated kinetic and photochemical data for atmospheric chemistry: Volume II - gas phase reactions of organic species, Atmos. Chem. Phys., 6, 3625-4055, 2006.

Baeza-Romero, M. T., Blitz, M. A., Goddard, A., and Seakins, P. W.: Time-of-flight mass spectrometry for time-resolved measurements: Some developments and applications, Int. J. Chem. Kinet., 44, 532-545, 10.1002/kin.20620, 2012.

Brune, W. H., Stevens, P. S., and Mather, J. H.: Measuring OH and HO_2 in the troposphere by laser-induced fluorescence at low-pressure, J. Atmos. Sci., 52, 3328-3336, 10.1175/1520-0469(1995)052<3328:moahit>2.0.co;2, 1995.

Cavalli, F., Geiger, H., Barnes, I., and Becker, K. H.: FTIR kinetic, product, and modeling study of the OH-initiated oxidation of 1-butanol in air, Environmental Science & Technology, 36, 1263-1270, 10.1021/es010220s, 2002.

Crowley, J. N., Simon, F. G., Burrows, J. P., Moortgat, G. K., Jenkin, M. E., and Cox, R. A.: The HO_2 radical UV absorption-spectrum measured by molecular modulation, UV diode-array spectroscopy, Journal of Photochemistry and Photobiology A-Chemistry, 60, 1-10, 10.1016/1010-6030(91)90001-a, 1991.

Dunlop, J. R., and Tully, F. P.: A kinetic study of OH radical reactions with methane and perdeuterated methane, J. Phys. Chem., 97, 11148-11150, 10.1021/j100145a003, 1993.

Edwards, G. D., Cantrell, C. A., Stephens, S., Hill, B., Goyea, O., Shetter, R. E., Mauldin, R. L., Kosciuch, E., Tanner, D. J., and Eisele, F. L.: Chemical ionization mass spectrometer instrument for the measurement of tropospheric HO_2 and RO_2, Anal. Chem., 75, 5317-5327, 10.1021/ac034402b, 2003.

Fuchs, H., Bohn, B., Hofzumahaus, A., Holland, F., Lu, K. D., Nehr, S., Rohrer, F., and Wahner, A.: Detection of HO_2 by laser-induced fluorescence: calibration and interferences from RO_2 radicals, Atmos. Meas. Tech., 4, 1209-1225, 10.5194/amt-4-1209-2011, 2011.

Gianella, M., Reuter, S., Aguila, A. L., Ritchie, G. A. D., and van Helden, J. P. H.: Detection of HO_2 in an atmospheric pressure plasma jet using optical feedback cavity-enhanced absorption spectroscopy, New Journal of Physics, 18, 10.1088/1367-2630/18/11/113027, 2016.

Glowacki, D. R., Goddard, A., Hemavibool, K., Malkin, T. L., Commane, R., Anderson, F., Bloss, W. J., Heard, D. E., Ingham, T., Pilling, M. J., and Seakins, P. W.: Design of and initial results from a highly instrumented reactor for atmospheric chemistry (HIRAC), Atmos. Chem. Phys., 7, 5371-5390, 2007.

Hanke, M., Uecker, J., Reiner, T., and Arnold, F.: Atmospheric peroxy radicals: ROXMAS, a new mass-spectrometric methodology for speciated measurements of HO_2 and ΣRO_2 and first results, International Journal of Mass Spectrometry, 213, 91-99, 10.1016/s1387-3806(01)00548-6, 2002.

Hard, T. M., O'Brien, R. J., Chan, C. Y., and Mehrabzadeh, A. A.: Tropospheric Free-radical determination by FAGE, Environmental Science & Technology, 18, 768-777, 1984.

Hurley, M. D., Wallington, T. J., Lauirsen, L., Javadi, M. S., Nielsen, O. J., Yamanaka, T., and Kawasaki, M.: Atmospheric Chemistry of n-Butanol: Kinetics, Mechanisms, and Products of Cl Atom and OH Radical Initiated Oxidation in the Presence and Absence of NOx, J. Phys. Chem. A, 113, 7011-7020, 10.1021/jp810585c, 2009.

Jemialade, A. A., and Thrush, B. A.: Reactions of HO_2 with NO and NO_2 studied by midinfrared laser magnetic-resonance, Journal of the Chemical Society-Faraday Transactions, 86, 3355-3363, 10.1039/ft9908603355, 1990.

McCaulley, J. A., Kelly, N., Golde, M. F., and Kaufman, F.: Kinetic studies of the reactions of F and OH with CH_3OH, J. Phys. Chem., 93, 1014-1018, 10.1021/j100340a002, 1989.

McGillen, M. R., Baasandorj, M., and Burkholder, J. B.: Gas-Phase Rate Coefficients for the OH plus n-, i-, s-, and t-Butanol Reactions Measured Between 220 and 380 K: Non-Arrhenius Behavior and Site-Specific Reactivity, J. Phys. Chem. A, 117, 4636-4656, 10.1021/jp402702u, 2013.

Medeiros, D. J., Blitz, M. A., James, L., Speak, T. H., and Seakins, P. W.: Kinetics of the Reaction of OH with Isoprene over a Wide Range of Temperature and Pressure Including Direct Observation of Equilibrium with the OH Adducts, J. Phys. Chem. A, 122, 7239-7255, 10.1021/acs.jpca.8b04829, 2018.

Monks, P. S.: Gas-phase radical chemistry in the troposphere, Chemical Society Reviews, 34, 376-395, 10.1039/B307982C, 2005.

Moore, S. B., and Carr, R. W.: Molecular velocity distribution effects in kinetic studies by time-resolved mass-spectrometry, Int. J. Mass Spectrom. Ion Processes, 24, 161-171, 10.1016/0020-7381(77)80023-5, 1977.

Onel, L., Brennan, A., Gianella, M., Ronnie, G., Aguila, A. L., Hancock, G., Whalley, L., Seakins, P. W., Ritchie, G. A. D., and Heard, D. E.: An intercomparison of HO_2 measurements by fluorescence assay by gas expansion and cavity ring-down spectroscopy within HIRAC (Highly Instrumented Reactor for Atmospheric Chemistry), Atmos. Meas. Tech., 10, 4877-4894, 10.5194/amt-10-4877-2017, 2017.

Orlando, J. J., Tyndall, G. S., Bilde, M., Ferronato, C., Wallington, T. J., Vereecken, L., and Peeters, J.: Laboratory and theoretical study of the oxy radicals in the OH- and Cl-initiated oxidation of ethene, J. Phys. Chem. A, 102, 8116-8123, 10.1021/jp981937d, 1998.

Orlando, J. J., Tyndall, G. S., and Wallington, T. J.: The atmospheric chemistry of alkoxy radicals, Chemical Reviews, 103, 4657-4689, 2003.

Reitz, R. D., and Duraisamy, G.: Review of high efficiency and clean reactivity controlled compression ignition (RCCI) combustion in internal combustion engines, Progress in Energy and Combustion Science, 46, 12-71, 10.1016/j.pecs.2014.05.003, 2015.

Stockwell, W. R., Lawson, C. V., Saunders, E., and Goliff, W. S.: A Review of Tropospheric Atmospheric Chemistry and Gas-Phase Chemical Mechanisms for Air Quality Modeling, Atmosphere, 3, 1, 2012.

Stone, D., Whalley, L. K., and Heard, D. E.: Tropospheric OH and HO_2 radicals: field measurements and model comparisons, Chem. Soc. Rev., 41, 6348-6404, 10.1039/c2cs35140d, 2012.

Stone, D., Blitz, M., Ingham, T., Onel, L., Medeiros, D. J., and Seakins, P. W.: An instrument to measure fast gas phase radical kinetics at high temperatures and pressures, Review of Scientific Instruments, 87, 054102, 2016.

Taatjes, C. A., and Oh, D. B.: Time-resolved wavelength modulation spectroscopy measurements of HO_2 kinetics, Appl. Opt., 36, 5817-5821, 10.1364/ao.36.005817, 1997.

Taatjes, C. A.: How does the molecular velocity distribution affect kinetics measurements by time-resolved mass spectrometry?, Int. J. Chem. Kinet., 39, 565-570, 10.1002/kin.20262, 2007.

Thiebaud, J., and Fittschen, C.: Near infrared cw-CRDS coupled to laser photolysis: Spectroscopy and kinetics of the HO_2 radical, Appl. Phys. B-Lasers Opt., 85, 383-389, 10.1007/s00340-006-2304-0, 2006.

Tully, F. P.: Laser photolysis laser-induced fluorescence study of the reaction of hydroxyl radical with ethylene, Chem. Phys. Lett., 96, 148-153, 10.1016/0009-2614(83)80481-3, 1983.

Whalley, L. K., Blitz, M. A., Desservettaz, M., Seakins, P. W., and Heard, D. E.: Reporting the sensitivity of laser-induced fluorescence instruments used for HO_2 detection to an interference from RO_2 radicals and introducing a novel approach that enables HO_2 and certain RO_2 types to be selectively measured, Atmos. Meas. Tech., 6, 3425-3440, 10.5194/amt-6-3425-2013, 2013.

Winiberg, F. A. F., Smith, S. C., Bejan, I., Brumby, C. A., Ingham, T., Malkin, T. L., Orr, S. C., Heard, D. E., and Seakins, P. W.: Pressure-dependent calibration of the OH and HO_2 channels of a FAGE HOx instrument using the Highly Instrumented Reactor for Atmospheric Chemistry (HIRAC), Atmos. Meas. Tech., 8, 523-540, 10.5194/amt-8-523-2015, 2015.

Zador, J., Taatjes, C. A., and Fernandes, R. X.: Kinetics of elementary reactions in low-temperature autoignition chemistry, Progress in Energy and Combustion Science, 37, 371-421, 10.1016/j.pecs.2010.06.006, 2011.